Available online at www.sciencedirect.com

ScienceDirect

IFAC PapersOnLine 52-5 (2019) 444–451

A Global Chassis Control System Involving Active Suspensions, Direct Yaw Control and Active Front Steering ⋆

A. Chokor * **R. Talj** * **M. Doumiati** ** **A. Charara** *

* *Sorbonne universités, Université de Technologie de Compiègne, CNRS, Heudiasyc UMR 7253, CS 60 319, 60 203 Compiègne, France.*
** *ESEO-IREENA EA 4642, 10 Bd Jeanneteau, 49100 Angers, France.*

Abstract: This paper aims to develop a Global Chassis Controller to coordinate the Active Front steering, Direct Yaw Control and Active Suspension controllers, in the ambition to improve the overall vehicle performance. A multilayer control architecture is adopted. It contains a local control layer and a decision layer. The local objectives for the sub-controllers in the control layer concern explicitly: maneuverability, lateral stability, rollover avoidance, and ride comfort. The sub-controllers are designed based on the super-twisting sliding mode theory. The decision layer is developed to promote/attenuate the local objectives of the sub-controllers, in order to remove the conflicts among the different objectives and extract the maximum benefit from the coordination using some evaluation criteria. This layer monitors the dynamics of the vehicle, calculates and sends scheduled gains to the sub-controllers, based on fuzzy logic rules and a stability criterion. Finally, the proposed Global Chassis Controller is validated on Matlab/Simulink using a vehicle model validated on the professional vehicle simulator "*SCANeR Studio*". The results show the effectiveness of the proposed strategy.

Keywords: Global Chassis Control; Multilayer Control; Super-Twisting Sliding Mode Control; Fuzzy Logic; Active Suspension; Direct Yaw Control; Active Front Steering.

1. INTRODUCTION

Driving safety is a major challenge for our society. According to the "National Highway Traffic Safety Administration (NHTSA)" statistics, human errors commit almost 90% of road accidents as explained in Rajamani (2012). The integration of an Advanced Driving Assistance System (ADAS) in the vehicle permits to act in an appropriate way to avoid accidents, skidding and rollover. ADAS systems are formed by several single-actuator approaches that have been proposed and marketed, such as: Vehicle Stability Control (VSC) or Electronic Stability Program (ESP) including Direct Yaw Control (DYC), Anti-lock Braking System (ABS) and others, to enhance the vehicle handling and stability; Active Front Steering (AFS) to improve the vehicle maneuverability or lane keeping; and Active Suspensions (AS) to improve comfort and road holding. Current and future intelligent vehicles are incorporating more sophisticated chassis control systems, known by Global Chassis Control system (GCC). GCC is an integrated vehicle chassis control system that coordinates several ADAS systems to improve the overall vehicle performance. It consists of creating a global performance efficient controller from sub-controllers which operate independently and have independent local objectives. Research in the GCC field mainly focus on the coordination of the AFS with the DYC, to improve the vehicle stability and maneuverability [Karbalaei et al. (2007)], [Poussot-Vassal et al. (2009)], and [Doumiati et al. (2013)]. The active (semi-active) suspensions were introduced in the GCC strategy to improve the ride comfort and road holding [Savaresi et al. (2010)], [Yoon et al. (2010)] and [Akhmetov et al. (2010)]. Recently, the GCC strategy has been evolved to coordinate different sub-controllers. Indeed, the studies on the active (semi-active) suspensions are enlarged to control the vehicle stability (lateral and vertical). Many research studies as Fergani et al. (2016), Chen et al. (2016), Vu et al. (2017), Yao et al. (2017), and Mirzaei and Mirzaeinejad (2017) propose to control the vertical load transfer when cornering, or minimizing the vertical displacements of the unsprung masses, known as the most influencing factors on the lateral tires forces, and thus on the lateral stability.

The main goal of the GCC system developed in this paper is to enhance the overall vehicle performance i.e. maneuverability, stability (lateral and vertical), and ride comfort. Fig. 1 depicts the general architecture of the proposed GCC. It consists of an AFS controller which will be developed to generate an additional steering angle, mainly to improve the maneuverability and enhance the lateral stability; a DYC controller which will be developed to generate a yaw moment that controls and guarantees the lateral stability of the vehicle; and an AS controller which will be developed to generate active suspension forces to improve ride comfort, vertical stability and lateral stability. The paper contributions are as follows:

- single-input single-output super-twisting sliding mode controllers are developed to control the active suspensions, the DYC, and the AFS in the presence of modeling errors, external disturbances and exogenous inputs.
- new objectives are achieved by the AS controller usually developed for ride comfort. It is exploited to improve the vertical stability (rollover avoidance) and lateral stability (lateral skidding avoidance). General improvements are

⋆ This work was supported by the Hauts-de-France Region and the European Regional Development Fund (ERDF).

10.1016/j.ifacol.2019.09.071

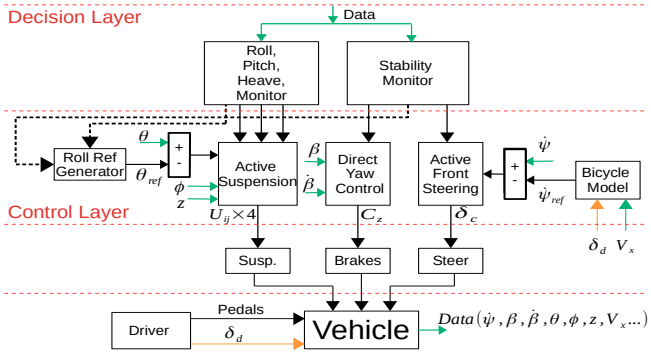

Fig. 1. Proposed GCC scheme

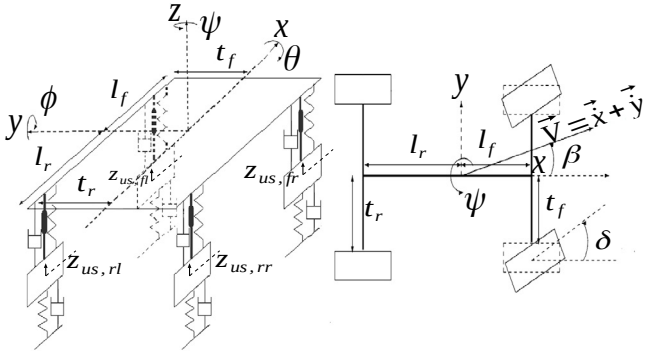

Fig. 2. Full vehicle model

Table 1. Nomenclature and vehicle parameters

Symbols	Description	Parameters values
CG	Vehicle center of gravity	
I_x	Roll moment of inertia of sprung mass	534 $[kg.m^2]$
I_z	Vehicle yaw moment of inertia	1970 $[kg.m^2]$
I_{xz}	Vehicle yaw-roll product of inertia	743 $[kg.m^2]$
h	Height of the vehicle CG	0.58 $[m]$
h_r	Height of the unsprung mass CG	0.31 $[m]$
h_θ	Sprung mass roll arm	0.27 $[m]$
M_s	Sprung mass	1126.4 $[kg]$
t_f	Half front track	0.773 $[m]$
t_r	Half rear track	0.773 $[m]$
l_f	Wheelbase to the front	1.0385 $[m]$
l_r	Wheelbase to the rear	1.6015 $[m]$
μ	Road adherence coefficient	dry surface= 1 $[-]$
C_f, C_r	Front, rear tire cornering stiffness	76776 $[N/rad]$
g	Gravity constant	9.81 $[m/s^2]$
i	$i = \{f : front, r : rear\}$	
j	$j = \{r : right, l : left\}$	
t	Time	[s]

also observed, e.g., the DYC will be less solicited, the vehicle speed will less drop, and others...

- development of a decision layer that promotes/attenuates the local sub-controllers objectives. This layer monitors the dynamics of the vehicle, calculates and sends scheduled gains to the sub-controllers, based on fuzzy logic rules and a stability criterion.

The paper structure is as follows: Section 2 develops the GCC system, starting by a review of the vehicle model, passing by the development of the sub-controllers to realize their local objectives and analyze the interactions between them, to finally develop the decision layer. Section 3 validates the proposed GCC system. Finally, the conclusions and the perspective works come in Section 4.

2. GLOBAL CHASSIS CONTROL SYSTEM

2.1 Vehicle model

A full vehicle nonlinear model has been already developed in Chokor et al. (2016). It combines the vertical, lateral, longitudinal, and tire/road contact (Dugoff model) sub-models, in addition to four wheels angular dynamics ω_{ij}, with a 26 state variables gathered in the state vector X of (1) and shown in Fig. 2. The vertical model describes the roll θ, pitch ϕ, heave z, and unsprung masses $z_{us,ij}$ (on four wheels) dynamics. The lateral model describes the lateral motion y (in the vehicle body frame), yaw motion ψ, and side slip β dynamics. Finally, the longitudinal model describes the longitudinal dynamics x (in the vehicle body frame). The vehicle parameters and variables are given in Table 1.

$$X = [\theta, \dot{\theta}, \phi, \dot{\phi}, z, \dot{z}, z_{us,ij}, \dot{z}_{us,ij}, \omega_{ij}, x, \dot{x}, y, \dot{y}, \psi, \dot{\psi}, \beta, \dot{\beta}]^T. \quad (1)$$

The full model has been validated in Chokor et al. (2017) for the so-called "*Family car*" vehicle using SCANeR Studio Simulator. *Family car* is a vehicle in SCANeR Studio Simulator that uses a very accurate vehicle model called *Callas vehicle model*, where the real dynamics are more detailed. In this section, essentials of the full model are given to show only the dynamics used to develop the GCC controller. These dynamics are given in Equations (2), (3), (4), (5) and (6). To be noted that equations (5) and (6) are linearized w.r.t the control input δ to facilitate their control. However, the GCC approach is validated on the Full vehicle model.

$$\ddot{\theta} = g_\theta(X) + f_\theta(X)M_\theta + d_\theta(X,t), \quad (2)$$

$$\ddot{\phi} = g_\phi(X) + f_\phi(X)M_\phi + d_\phi(X,t), \quad (3)$$

$$\ddot{z} = g_z(X) + f_z(X)M_z + d_z(X,t), \quad (4)$$

$$\ddot{\psi} = g_\psi(X) + f_{\psi,\delta}(X)\delta + f_{\psi,C_z}(X)C_z + d_\psi(X,t), \quad (5)$$

$$\ddot{\beta} = g_\beta(X) + f_{\beta,\delta}(X)\delta + f_{\beta,C_z}(X)C_z + d_\beta(X,t). \quad (6)$$

M_θ, M_ϕ, and M_z represent respectively the active roll moment, active pitch moment, and active heave force, as intermediate control inputs. These inputs have to be generated at a lower level control by physical actuators, e.g. Active Suspensions AS forces U_{ij} integrated on four corners. $\delta = \delta_d + \delta_c$ is the total steering angle at the front wheels, where δ_d is the one provided by the driver and δ_c is the one provided by the AFS controller. C_z is the active yaw torque provided by the DYC controller. C_z has to be generated at a lower level control as a differential braking on the rear wheels. $g_q(X)$, $f_v(X)$, $f_{l,\delta}(X)$, and $f_{l,C_z}(X)$ where $q = \{v,l\}$, $v = \{\theta,\phi,z\}$ and $l = \{\psi,\beta\}$ are nonlinear continuous functions detailed in Appendix A. $d_q(X,t)$ represent modeling errors and external disturbances supposed to be bounded as given in (7).

$$|d_q(X,t)| \leq D_q;\ q = \{\theta,\phi,z,\psi,\beta\}, \quad (7)$$

where D_q are positive constant values.

Note:1

-The lateral and longitudinal accelerations used later in the paper are in a fixed reference frame and are noted respectively by a_y and a_x. In modeling, a_y and a_x are constructed from $\dot{x}$, $\ddot{x}$, $\dot{y}$, $\ddot{y}$, $\dot{\psi}$. V_x used later in the paper is the time integral of a_x.

-In real time control, the controlled variables $\dot{\psi}$, $\dot{\phi}$ and $\dot{\theta}$ are measured by gyrometers and provided at the CG of the vehicle. θ and ϕ are estimated by time integration and could be provided by the Inertial Measurement Unit IMU -if available-. a_y, a_x and $\ddot{z}$ are measured by accelerometers. $\dot{z}$, z are integrated from $\ddot{z}$. The side slip angle β and its derivative $\dot{\beta}$ could be estimated. Several observer approaches that suit the real time constraints implementation and vehicle dynamics have been proposed in

literature to estimate β and $\dot{\beta}$, e.g. an Extended Kalman Filter EKF based observer as done in Chen et al. (2016).

2.2 GCC sub-controllers

In order to develop robust individual controllers for the sub-systems described by Equations (2), (3), (4), (5) and (6), dealing with the nonlinear behavior of the vehicle, and in the presence of unmodeled dynamics, external disturbances and exogenous inputs (for some cases), the super-twisting second order sliding mode theory as a robust model-based theory is chosen to control the sub-controllers AS, AFS, and DYC.

a) Super-twisting sliding mode controller:
In this Subsection, an overview of the super-twisting sliding mode control theory is presented. Used notations refers only to this subsection, unless mentioned in the other subsections.
The super-Twisting algorithm is a second order sliding mode control that handles a relative degree equal to one. It generates the continuous control function that drives the sliding variable and its derivative to zero in finite time in the presence of smooth matched disturbances.
Consider the system written as:

$$\dot{x} = f(x,t) + g(x,t)u(t) \tag{8}$$

where u is the control input, $x \in \Re^n$ the state vector, and f, g continuous functions. Let us define a sliding variable s of relative degree equal to one, and with a second derivative written as:

$$\ddot{s}(s,t) = \Phi(s,t) + \xi(s,t)\dot{u}(t) \tag{9}$$

where $\Phi(s,t)$ and $\xi(s,t)$ are unknown bounded signals.
The control objective is to achieve the convergence to the sliding surface defined as $s = 0$. Only the knowledge of s is required in real time.
Suppose that there exist positive constants S_0, b_{min}, b_{max}, C_0, U_{max} such that $\forall x \in \Re^n$ and $|s(x,t)| < S_0$, the system satisfies the following conditions:

$$\begin{cases} |u(t)| \leq U_{max} \\ |\Phi(s,t)| < C_0 \\ 0 < b_{min} \leq |\xi(s,t)| \leq b_{max} \end{cases} \tag{10}$$

The sliding mode control law, based on the Super-Twisting algorithm, is given by:

$$u(t) = u_1 + u_2 \begin{cases} u_1 = -\alpha_1 |s|^{\tau} \text{sign}(s), \ \ \tau \in]0, 0.5] \\ \dot{u}_2 = -\alpha_2 \text{sign}(s) \end{cases} \tag{11}$$

α_1 and α_2 are positive gains. The finite time convergence is guaranteed by the following conditions:

$$\begin{cases} \alpha_1 \geq \sqrt{\frac{4C_0(b_{max}\alpha_2 + C_0)}{b_{min}^2(b_{min}\alpha_2 - C_0)}} \\ \alpha_2 > \frac{C_0}{b_{min}} \end{cases} \tag{12}$$

The convergence analysis is shown in Utkin (2013).

b) AS controller structure:
The common objectives of the active suspensions widely developed in literature are improving the ride comfort and road holding [Savaresi et al. (2010)], [Yoon et al. (2010)] and [Akhmetov et al. (2010)]. One objective of this paper is to emphasize new achievable enhancements on the global chassis performance through the coordinated integration of the active suspensions. These enhancements concern directly the rollover and the lateral stability. Hence, the other sub-controllers in the GCC structure become less solicited, and consequently, the safe vertical and lateral ranges of the vehicle manipulation can be enlarged

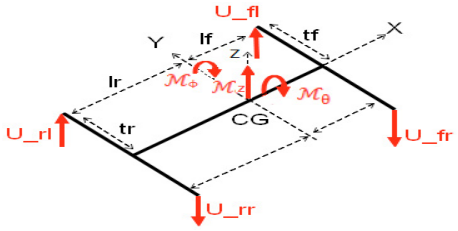

Fig. 3. Active forces distribution

to more hard maneuvers. Let first develop an AS controller dedicated to ride comfort. The concerned dynamics of ride comfort are the roll, pitch and heave motions of the sprung mass, developed respectively in Equations (2), (3) and (4). A general form of these dynamics can be written as:

$$\ddot{v} = g_v(X) + f_v(X)M_v + d_v(X,t). \tag{13}$$

Each of these equations has a unique control input M_v, that acts only on the corresponding variable v. Thus, similar controllers with particular gains can be developed for all of these dynamics. To control these dynamics, one can choose the super-twisting sliding mode control law known by its robustness to modeling errors and external disturbances. Let $v_{des} = \{\theta_{des}, \phi_{des}, z_{des}\}$ be the desired states and $\dot{v}_{des} = \{\dot{\theta}_{des}, \dot{\phi}_{des}, \dot{z}_{des}\}$ be their time derivatives. Then, let:

$$e_v = v - v_{des}, \tag{14}$$

be the error between the actual and desired states. Let:

$$s_v = \dot{e}_v + \lambda_v \, e_v, \tag{15}$$

be the sliding variable, chosen with a relative degree of 1 w.r.t the control input M_v (the control input appears in the first time derivative of the sliding variable) to meet the super-twisting constraints. This means that the discontinuous function appears in the second derivative of the sliding variable such that:

$$\ddot{s}_v(s_v,t) = \Phi_v(s_v,t) + \xi_v(s_v,t)\dot{M}_v(t), \tag{16}$$

where $\Phi_v(s_v,t)$ and $\xi_v(s_v,t)$ are unknown bounded functions satisfying conditions of (10).
The sliding mode control input, based on the Super-Twisting algorithm, is given by:

$$M_v(t) = -\alpha_{v,1}|s_v|^{\tau_v} sign(s_v) - \alpha_{v,2}\int_0^t sign(s_v)d\tau, \tag{17}$$

where $\alpha_{v,1}$ and $\alpha_{v,2}$ are positive gains satisfying conditions of (12), and $\tau_v \in]0, 0.5]$.
The super-twisting algorithm guaranties the convergence of s_v in a finite time to zero. Once $s_v = 0$, the states v and $\dot{v}$ exponentially converge to v_{des} and $\dot{v}_{des}$ respectively if $\lambda_v > 0$. The function *sign* is smoothed by the approximation $sign(s_v) = \frac{s_v}{|s_v| + \varepsilon_v}$, where $\varepsilon_v > 0$.
Once the needed control inputs M_θ, M_ϕ, and M_z are obtained to control θ, ϕ, and z, there are different ways to generate them by the active suspension forces on the four vehicle corners. For simplicity, one suggests generating each needed control input by doing a geometrical distribution between the four suspensions as given in (18) (see Fig. 3).

$$\begin{aligned} U_{fl} &= 0.5\frac{l_r}{l_f+l_r}\frac{M_\theta}{t_f} - 0.5\frac{M_\phi}{l_f+l_r} + 0.5\frac{l_r}{l_f+l_r}M_z, \\ U_{fr} &= -0.5\frac{l_r}{l_f+l_r}\frac{M_\theta}{t_f} - 0.5\frac{M_\phi}{l_f+l_r} + 0.5\frac{l_r}{l_f+l_r}M_z, \\ U_{rl} &= 0.5\frac{l_f}{l_f+l_r}\frac{M_\theta}{t_r} + 0.5\frac{M_\phi}{l_f+l_r} + 0.5\frac{l_f}{l_f+l_r}M_z, \\ U_{rr} &= -0.5\frac{l_f}{l_f+l_r}\frac{M_\theta}{t_r} + 0.5\frac{M_\phi}{l_f+l_r} + 0.5\frac{l_f}{l_f+l_r}M_z. \end{aligned} \tag{18}$$

The objective of ride comfort in literature is to minimize the roll, pitch and heave angles and velocities/accelerations [Savaresi et al. (2010)], [Yoon et al. (2010)] and [Akhmetov et al. (2010)], thus, $v_{des} = \dot{v}_{des} = \{0,0,0\}$.
Now, the AS control task will be extended to consider the objective of rollover avoidance (vertical stability). The rollover phenomenon starts to happen when the vehicle lateral acceleration exceeds a certain value called the maximal safe lateral acceleration developed in Chokor et al. (2017), which depends on the constant vehicle geometry ratio t_f/h and the roll angle as expressed in (19):

$$a_{y_{safe}} = 0.7\frac{sign(a_y)t_f - (h-h_r)\theta}{h}g. \quad (19)$$

A lateral acceleration a_y above $a_{y_{safe}}$ risks the vehicle inner wheels to lift off when cornering. To avoid the rollover, the lateral acceleration a_y should be maintained below this threshold. By minimizing the roll angle, the maximal safe lateral acceleration $a_{y_{safe}}$ can be elevated, and thus, prevent the rollover. Accordingly, turning the roll angle in the opposite direction (to the inner side of the corner) will shift $a_{y_{safe}}$ more towards a higher value. From our point of view, turning the roll angle towards the inner wheels when cornering reassures the driver and gives him the confidence of piloting the vehicle. The choice of the desired roll angle θ_{des} is done as follows:
- For $a_y = 0$ (straight road), the desired roll angle is 0°.
- For $a_y = 0.7\frac{t_f}{h}g$ (maximal safe lateral acceleration threshold), the desired roll angle is equal to the maximal achievable roll angle 10° (vehicle design constraints).
- The map between θ_{des} and a_y is supposed to be linear to make a smooth comfortable roll rate of change.
Thus, the desired roll angle θ_{des} is given in (20):

$$\theta_{des} = -\frac{10\frac{\pi}{180}}{0.7\frac{t_f}{h}g}a_y. \quad (20)$$

c) AFS controller structure:
Maneuverability or steer-ability means having a linear relation between the steering provided by the driver and the achieved vehicle yaw rate. The objective of the AFS controller is to enhance the steer-ability, thus, converging the real vehicle yaw rate to a desired one linear to the steer angle provided by the driver. The linear relation can be derived from a linear vehicle model called *"bicycle model"* [Rajamani (2012)] which represents a stable and ideal motion of the vehicle, where the lateral tires forces are supposed to be linear to the tires side slip angles. The bicycle model is given in (21):

$$\begin{pmatrix}\ddot{\psi}_{ref}\\ \dot{\beta}_{ref}\end{pmatrix} = \begin{bmatrix}-\mu\frac{l_f{}^2c_f+l_r{}^2c_r}{I_zV_x} & \mu\frac{l_rc_r-l_fc_f}{I_z}\\ -1+\mu\frac{l_rc_r-l_fc_f}{MV_x{}^2} & -\mu\frac{c_f+c_r}{MV_x}\end{bmatrix}\begin{pmatrix}\dot{\psi}_{ref}\\ \beta_{ref}\end{pmatrix} + \begin{bmatrix}\mu\frac{l_fc_f}{I_z}\\ \mu\frac{c_f}{MV_x}\end{bmatrix}\delta_d, \quad (21)$$

where δ_d is the driver steer angle on the front wheels, $\dot{\psi}_{ref}$ is the ideal reference yaw rate, β_{ref} is the corresponding side slip angle, and V_x is the vehicle longitudinal speed. As the lateral stability is related to the lateral acceleration a_y, the authors in Rajamani (2012) propose to maintain a_y below a threshold depending on the maximal possible adherence (22), by saturating $\dot{\psi}_{ref}$, as described in (23).

$$a_y \simeq V_x(\dot{\psi}+\dot{\beta}) \leq \mu\, g, \quad (22)$$

$$\dot{\psi}_{ref,max} = 0.85\mu\, g/V_x. \quad (23)$$

The objective of the AFS is thus to converge the measured yaw rate $\dot{\psi}$ whose dynamics is described in (5) to the saturated reference $\dot{\psi}_{ref}$, to enhance the maneuverability in the framework of the lateral stability. This can be done by adjusting the driver steering angle δ_d through the introduction of the corrective term δ_c as the AFS control input calculated based on the super-twisting Sliding Mode control theory. δ_d and C_z are treated as exogenous inputs to the yaw dynamics of (5). Both exogenous inputs are bounded and supposed to be constants at each iteration.The value of δ_d is supposed to be measured by a sensor, while the value of C_z is taken from the precedent iteration since it is not calculated yet.
Let define the sliding variable as follows:

$$s_\psi = e_\psi = \dot{\psi} - \dot{\psi}_{ref}. \quad (24)$$

The variable s_ψ has a relative degree of 1 w.r.t the control input δ_c. Thus,

$$\ddot{s}_\psi(s_\psi, C_z, \delta_d, t) = \Phi_\psi(s_\psi, C_z, \delta_d, t) + \xi_\psi(s_\psi, C_z, \delta_d, t)\dot{\delta}_c(t). \quad (25)$$

$\Phi_\psi(s_\psi, C_z, \delta_d, t)$ and $\xi_\psi(s_\psi, C_z, \delta_d, t)$ are unknown bounded functions satisfying conditions of (10). By the same reasoning used above, the super-twisting control input δ_c can be formulated as (26):

$$\delta_c = -\alpha_{\psi,1}\left|s_\psi\right|^{\tau_\psi} sign(s_\psi) - \alpha_{\psi,2}\int_0^t sign(s_\psi)d\tau. \quad (26)$$

This algorithm guarantees the convergence of s_ψ to zero in a finite time, if the gains $\alpha_{\psi,1}$ and $\alpha_{\psi,2}$ satisfy the same convergence conditions of (12), and $\tau_\psi \in]0,\, 0.5]$.
This control strategy enhances the maneuverability of the vehicle and maintain the lateral acceleration below the lateral-skidding threshold $\mu.g$, where μ is the road adherence coefficient and g is the gravity constant as discussed in Rajamani (2012). However, the lateral stability also depends on the vehicle side slip angle and its rate of change. Thus, this control strategy enhances without guarantee the lateral stability, especially when these variables are solicited enough to destabilize the vehicle. To resolve the problem, the first intuitive solution is to introduce the control of β and $\dot{\beta}$ in the objectives of the AFS controller. However, the yaw torque provided by the steering in the critical range of lateral stability is not enough to stabilize the vehicle since the lateral tires forces will be saturated. Alternatively, the DYC controller using differential rear braking is known to be effective to control β and $\dot{\beta}$, while it has the disadvantages of: decelerating the vehicle, long-term wheels wear, and driver discomfort. Thus, it is recommended to actuate the DYC controller only under critical situations.

d) DYC controller structure:
The objective of the DYC controller is to minimize the side slip angle β and its rate of change $\dot{\beta}$ when the vehicle is under critical driving situations by generating an active yaw moment. The physical actuators to create the yaw moment are selected to be the rear electro-mechanical brakes. This choice prevents direct interference with the active steering on the front tires [Doumiati et al. (2013)]. In this subsection, the DYC controller will be developed as a decentralized controller, i.e. to control β and $\dot{\beta}$ whatever the driving situation is. Later, in the coordination layer, the DYC controller will be activated based on a decision rule.
Similar to the case of the AFS, the super-twisting sliding mode control law is adopted to control β and $\dot{\beta}$, while the control input of the DYC is the additive yaw torque C_z. δ is treated as the exogenous input, it is available, bounded and supposed constant at the time iteration. Let the sliding variable be:

$$s_\beta = \beta + \lambda_\beta\, \dot{\beta}. \quad (27)$$

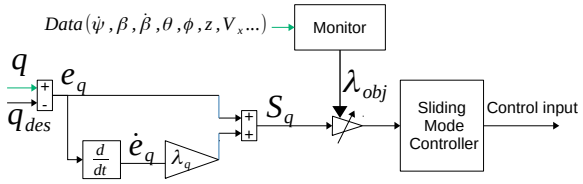

Fig. 4. Scheduled controller

The sliding variable has a relative degree of 1 w.r.t the control input C_z . By the same reasoning as before, the super-twisting algorithm guarantees the convergence of s_β to zero in a finite time. Thus, β and $\dot{\beta}$ converge exponentially to zero if $\lambda_\beta > 0$. Finally, the super twisting sliding mode control input C_z is given in (28) by:

$$C_z = -\alpha_{\beta,1} \left|s_\beta\right|^{\tau_\beta} sign(s_\beta) - \alpha_{\beta,2} \int_0^t sign(s_\beta) d\tau, \qquad (28)$$

where $\alpha_{\beta,1}$ and $\alpha_{\beta,2}$ satisfy conditions of (12), and $\tau_\beta \in]0, 0.5]$.

2.3 GCC architecture

Based on the above analysis, a decision layer will be developed in this section to coordinate the proposed sub-controllers. The main idea is to promote/attenuate the control objective by multiplying each sliding variable by a scheduled gain $\{\lambda_{obj}\} = \{\lambda_{AFS}, \lambda_{DYC}, \lambda_{AS_{Roll}}, \lambda_{AS_{Pitch}}, \lambda_{AS_{Heave}}\}$ as depicted in Fig. 4. The decision layer monitors all controllers objectives based on monitoring criteria (data) and a set of coordination rules defined in the following, then, it calculates and sends instantly the exact value of λ_{obj} to attenuate/promote the corresponding objective. Each of λ_{obj} varies between 0 and 1. As much λ_{obj} approaches to 1, as the control objective is promoted, vice versa, the control objective is completely attenuated when λ_{obj} approaches to 0. From a control point of view, the proof of maintaining the total stability of the global system when injecting these scheduled gains is not given is this paper. Further investigations will be done in future works to demonstrate this issue.

AFS and DYC coordination rules:
The criteria by which the lateral stability can be quantified is called "*lateral stability index (SI)*". SI reflects the orientation of the vehicle w.r.t its speed vector at the *CG*, and its rate of change. The lateral stability index (SI) used in Chen et al. (2016) is expressed in (29) as:

$$SI = \left|2.49\dot{\beta} + 9.55\beta\right|. \qquad (29)$$

For $SI \leq \underline{SI}$ (a predefined threshold depending on the vehicle and road parameters), the vehicle is in normal driving situations, else, the vehicle reaches critical driving conditions (the vehicle has to be controlled to come back to the normal driving situation before losing stability). * If the vehicle situation is normal $SI \leq \underline{SI}$, then the AFS controller should be promoted to improve the maneuverability. In this range, the DYC controller is disabled.
* If the vehicle is under critical situation $SI \geq \underline{SI}$, then the DYC controller should be promoted to enhance the lateral stability. In this range, the AFS controller has a poor effect to enhance the lateral stability, thus, it may not be actuated.
* To ensure a smooth switch between the controllers, the switching condition will be enlarged to a range of *SI*, such a range is between two thresholds: $\underline{SI} = 0.6$ (low threshold) and $\overline{SI} = 0.8$ (high threshold). These thresholds are chosen based on

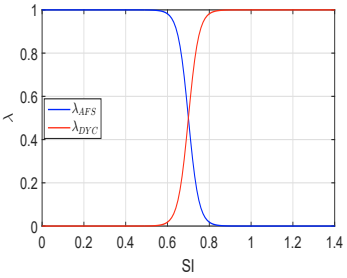

Fig. 5. Switching function of AFS and DYC

the simulation results for the used vehicle and road parameters. The AFS and DYC will be attenuated/promoted smoothly and continuously in this range as seen in Fig. 5. The switching function is a "*sigmoid function*". The scheduled gains are given in (30) as:

$$\lambda_{DYC} = \frac{1}{1+e^{-\frac{8}{\overline{SI}-\underline{SI}}(SI-\frac{\overline{SI}+\underline{SI}}{2})}}, \qquad \lambda_{AFS} = 1 - \lambda_{DYC}. \qquad (30)$$

Active suspension (AS) coordination/actuation rules:
The proposed AS controller will participate in the GCC by achieving three main objectives: roll control, pitch control and heave control. To reduce the excessive actuation of the AS (AS relaxation), while maintaining good ride and stability (vertical and lateral) qualities, the following supervision rules will promote/attenuate these objectives:
- Roll control objective: As we believe that turning the roll angle in the opposite direction improves driver comfort, thus, the roll objective can always be oriented to achieve $\theta = \theta_{des}$ expressed in (20). By this procedure, the ride comfort (in terms of roll motion) and the stability (lateral and vertical) will be enhanced regardless of *SI*. Thus, $\lambda_{AS_{Roll}} = 1$ whatever the vehicle situation is.
-The Pitch control objective has to be attenuated/promoted depending on the severity of braking/acceleration, to reduce the use of the AS while maintaining good ride quality (in terms of pitch motion). Thus, only the harsh and considerable pitch motion has to be minimized, indeed, $\lambda_{AS_{Pitch}}$ approaches to 1 to promote the pitch control objective. As much the pitch motion becomes soft, as $\lambda_{AS_{Pitch}}$ will approach more to 0 to attenuate the pitch control objective.
One suggests treating $\lambda_{AS_{Pitch}}$ as a fuzzy-scheduled gain $\lambda_{AS_{Pitch}}$ which attenuates/promotes the pitch control objective, based on the pitch angle error (14) and its rate of change. The pitch angle error and its rate of change are applied to the Fuzzy Logic Controller (FLC) as inputs, and the fuzzy-scheduled gain $\lambda_{AS_{Pitch}}$ is the output. The reason of choosing the FLC for the decision-making process is due to its simplicity to make the relation between the needed control input and the controlled variables in an intuitive way. Five fuzzy sets are defined for each input, and three for the output: $\{e_\phi, \dot{e}_\phi\} = \{NB\ (Negative\ Big),\ NS\ (Negative\ Small),\ ZE\ (Zero),\ PS\ (Positive\ Small),\ PB\ (Positive\ Big)\}$; $\{\lambda_{AS_{Pitch}}\} = \{PS,\ PM\ (Positive\ Medium),\ PB\}$. The normalized Membership Functions (MFs) of fuzzification of the controller inputs and defuzzification of the controller output are respectively given in Figs. 6a, 6b and 7. To determine the fuzzy controller output $\lambda_{AS_{Pitch}}$ for the given fuzzy controller inputs e_ϕ and $\dot{e}_\phi$, the decision matrix of the linguistic control rules is designed and presented in Table 2. These fuzzy sets, membership functions,

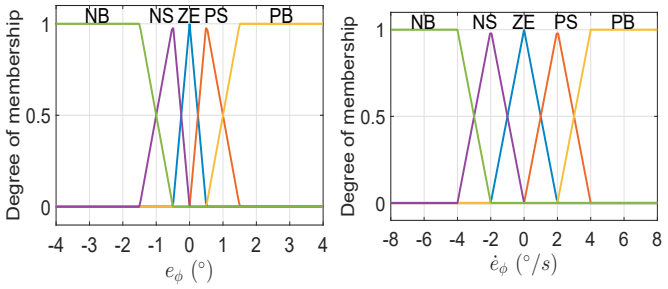

(a) Fuzzy sets - input 1

(b) Fuzzy sets - input 2

Fig. 6. Fuzzy sets of the inputs

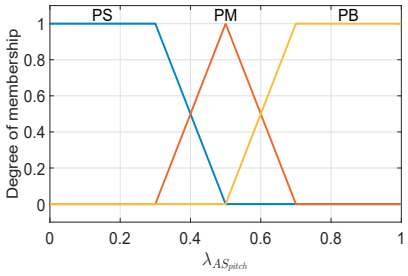

Fig. 7. Fuzzy sets of the output

Table 2. Fuzzy rules of $\lambda_{AS_{Pitch}}$

$\lambda_{AS_{Pitch}}$		$\dot{\mathbf{e}}_\phi$				
		NB	**NS**	**ZE**	**PS**	**PB**
$\mathbf{e}_\phi$	**NB**	PB	PB	PM	PM	PS
	NS	PB	PM	PS	PS	PM
	ZE	PM	PS	PS	PS	PM
	PS	PM	PS	PS	PM	PB
	PB	PS	PM	PM	PB	PB

and the linguistic rules are usually determined based on an expert knowledge of the system by performing several simulations. Finally, to defuzzify the result/output, the "*Mamdani centroid fuzzy inference method*" is used [Reznik (1997)].

- Heave control objective attenuation/promotion is done in a similar manner to the pitch control objective. That means, a fuzzy-scheduled gain $\lambda_{AS_{Heave}}$ is obtained to regulate the degree of achievement of the heave control objective depending on the harshness of this motion.

3. GCC VALIDATION AND SIMULATION

In this section, the proposed GCC system will be validated through two simulation tests (presented later) using Matlab/Simulink. The simulation model of the full vehicle is developed and validated on the professional vehicle simulator "*SCANeR Studio*" [Chokor et al. (2016)] and [Chokor et al. (2017)].
The first test is a sine steer (Fig. 8) at 100 km/h initial speed. This test solicits the vehicle yaw and lateral motions, as well as the roll motion. The uncontrolled (induced), desired and controlled roll angles are shown in Fig. 9. The lateral Stability Index SI, without controlling the vehicle, increases to reach more than $SI = 1$ as shown in Fig. 10. That means, the vehicle has lost its lateral stability. The AFS controller alone (dedicated to the maneuverability) could diminish the SI to 1 as shown in the same figure. However, this improvement is not sufficient. The coordinated AFS and DYC controller could maintain the lateral stability under $SI = 0.8$. This improvement is obtained thanks to

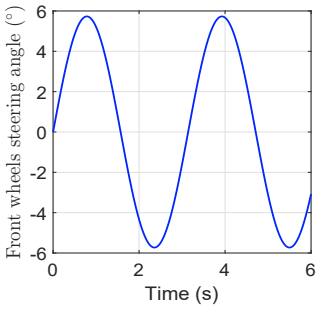

Fig. 8. Front wheels steering

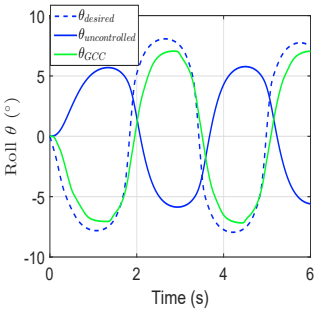

Fig. 9. Roll angle control

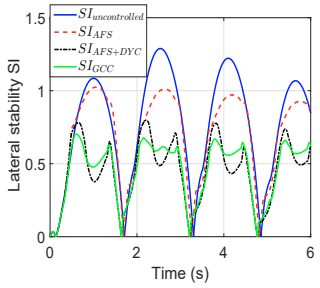

Fig. 10. Lateral Stability Index

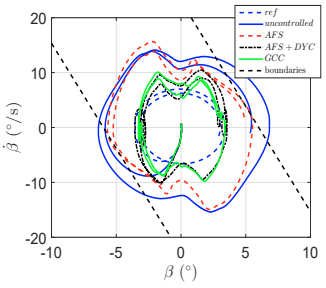

Fig. 11. β-$\dot{\beta}$ phase plane

the torque C_z generated by the DYC that stabilizes the side slip angle β and its rate of change $\dot{\beta}$. The addition of the roll control to the GCC structure (by the AS) could enhance more the lateral stability by diminishing the peak value of SI ($SI = 0.8$) to less than 0.7. The lateral stability can be alternatively studied in the "$\beta - \dot{\beta}$ *phase plane*" shown in Fig. 11. The boundaries are for $SI = 1$. As much $\beta - \dot{\beta}$ relation is near the ideal one -calculated from the bicycle reference model-, as the lateral stability is more enhanced. It can be noticed that the uncontrolled vehicle exceeds the boundaries, while the GCC controller is the nearest one to $\beta - \dot{\beta}$ reference. The vehicle yaw rate is shown in Fig. 12. In the ranges below the saturation of the yaw rate reference, the uncontrolled vehicle is somehow far away from the yaw rate reference. Meanwhile, all the adopted strategies (AFS, AFS + DYC, and the GCC) converge to the desired yaw rate. This means that the maneuverability is enhanced regardless of the adopted strategy. When the vehicle yaw rate becomes too much high, the control objective attempts to saturate the yaw rate in order to simultaneously enhance the lateral stability and avoid the nonlinear relation between the yaw rate and the driver steering. The AFS is shown to be the most effective controller in making the vehicle yaw rate converges to the desired saturated one. The DYC, by the braking effect to stabilize the vehicle, tends to diminish its kinetic energy, which is reflected by a reduction of the yaw rate. When adding the roll control (by means of AS) to the GCC system to enhance the stability, the DYC controller becomes less solicited, and thus, the yaw rate re-approaches to the desired one.
To evaluate the rollover risk, the Load Transfer Ratio (LTR) used in Rajamani (2012) and described in (31) is evaluated.

$$LTR = \frac{F_{z_r} - F_{z_l}}{F_{z_r} + F_{z_l}}, \tag{31}$$

where F_{z_r} and F_{z_l} are the vertical forces on the right and left side wheels respectively. The rollover is supposed to start when the vehicle inner wheels lift off from the ground. Thus, the rollover starts when F_{z_l} or F_{z_r} becomes zero, which means all the load

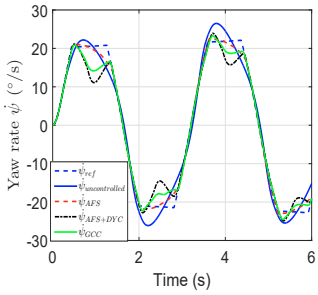

Fig. 12. Yaw rate comparison

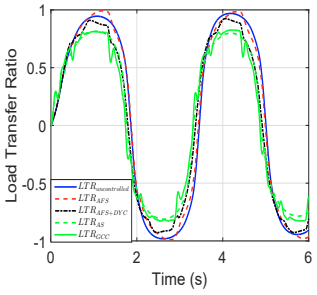

Fig. 13. Load Transfer Ratio

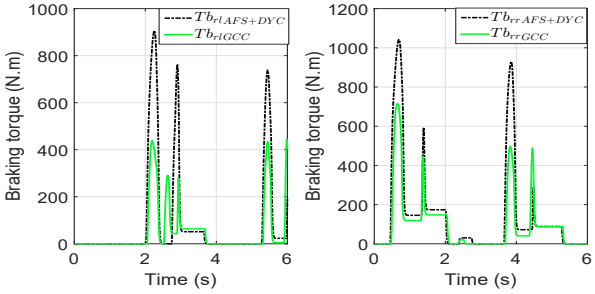

Fig. 14. Active Brake torques

is on the outer wheels. Hence, it occurs when the $LTR = \pm 1$. Figure 13 shows the LTR of the uncontrolled vehicle and the different control strategies. The results show that the LTR is the best when the GCC strategy is adopted compared to other strategies. It can also be noticed that activating the AFS alone has a drawback on the LTR. The fact is because the vertical stability is not considered in the development of the AFS controller.

Divers comfort enhancements are noticed when adding the roll control to the GCC system. One observes that:

- The active differential braking on the rear wheels, provided by the DYC controller to stabilize the vehicle, are reduced as shown in Fig. 14. The justification is that the AS contributes to the stabilization process. According to the same figure, the Root Mean Square RMS of the braking torques are reduced by 47% on the rear left wheel and by 36% on the rear right wheel. The RMS reflects the dissipated energy by the braking actuator, which has an impact on its life time. The peak values of both braking are also considerably diminished by 53% and 30% respectively.
- The vehicle speed drop caused by the braking is less reduced as shown in Fig. 15.
- The critical longitudinal slipping of the rear tires caused by the differential braking are limited as shown in Fig. 16. Consequently, the ABS control system (supposed to be integrated into the chassis) will be less solicited. The second test represents a smooth medium accelerating followed by a sharp and hard braking as shown in Fig. 17. The smooth/sharp acceleration/braking solicits the pitch rate, while the medium/hard value solicits the pitch angle, which are respectively represented by the uncontrolled vehicle in Figs. 18a and 18b. The AS controller eliminates the pitch angle and rate motion almost entirely, while the GCC controller only diminishes the high values of the pitch angle and rate to ensure a soft pitch motion. The control inputs of the four AS are depicted in Fig. 19. The RMS value of the total input is diminished by 22%.

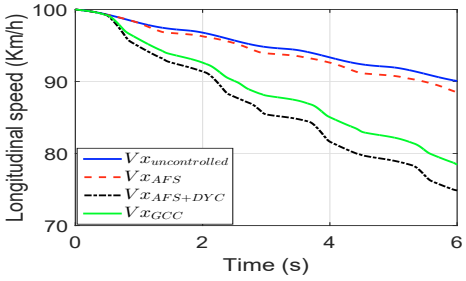

Fig. 15. Longitudinal speed

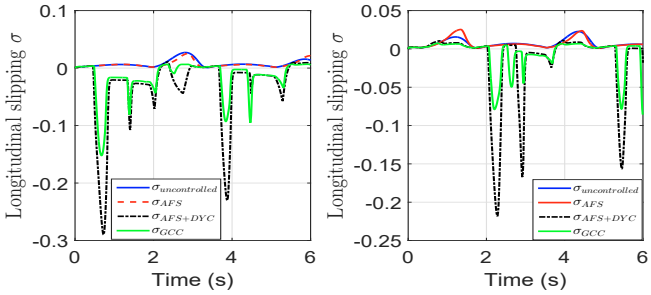

Fig. 16. Longitudinal slipping

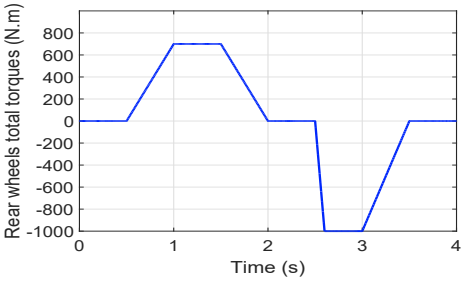

Fig. 17. Total driver torques on rear wheels

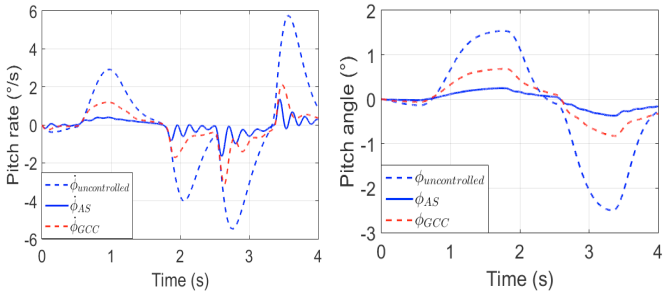

(a) Pitch rate comparison (b) Pitch angle comparison

Fig. 18. Pitch motion comparison

4. CONCLUSION AND PERSPECTIVES

In this paper, a Multilayer GCC system that coordinates the AFS, DYC, and AS has been developed. It consists of a decision layer and control layer. The decision layer supervises the control layer which contains three main sub-controllers (AFS, DYC, and AS) dedicated to improve local performances. The supervision can be divided into two categories: 1− monitor the overall vehicle performance by coordinating the interactions between the different control objectives (reinforce the favorable interactions and restrain the detrimental ones); 2− reduce the

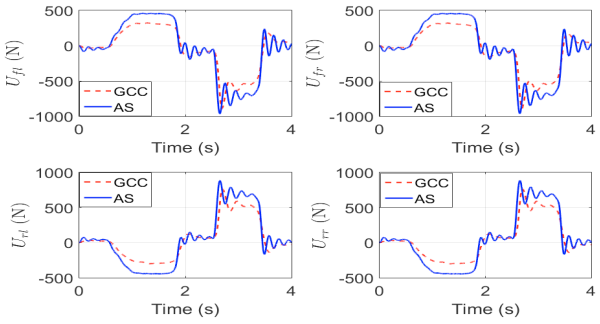

Fig. 19. AS control inputs comparison

use of the AS to involve only the undesirable motions of ride comfort. The GCC strategy has been validated by simulation results. As a part of the future work, beside the proof of maintaining the total stability of the system when injecting these scheduled gains, the proposed GCC will be evolved to integrate more interactions, objectives, and sub-controllers. Studies will also focus on the development of a fault tolerant GCC system.

ACKNOWLEDGEMENTS

The authors would like to thank the Hauts-de-France Region and the European Regional Development Fund (ERDF) 2014/2020 for the funding of this work, through the SYSCOVI project. This work was also carried out in the framework of the Labex MS2T, (Reference ANR-11-IDEX-0004-02) and the Equipex ROBOTEX (Reference ANR-10-EQPX-44-01) which were funded by the French Government, through the program "Investments for the future" managed by the National Agency for Research.

REFERENCES

Akhmetov, Y., Rémond, D., Maiffredy, L., Di Loreto, M., Marquis-Favre, W., and Harth, V. (2010). Global Chassis Control for active safety of heavy vehicles. In *World Automotive Congress FISITA*, F2010–D–057.

Chen, W., Xiao, H., Wang, Q., Zhao, L., and Zhu, M. (2016). *Integrated vehicle dynamics and control*. John Wiley & Sons.

Chokor, A., Talj, R., Charara, A., Doumiati, M., and Rabhi, A. (2017). Rollover prevention using active suspension system. In *20th International Conference on Intelligent Transportation Systems (ITSC)*, 1706–1711. IEEE.

Chokor, A., Talj, R., Charara, A., Shraim, H., and Francis, C. (2016). Active suspension control to improve passengers comfort and vehicle's stability. In *19th International Conference on Intelligent Transportation Systems (ITSC)*, 296–301. IEEE.

Doumiati, M., Sename, O., Dugard, L., Martinez-Molina, J.J., Gaspar, P., and Szabo, Z. (2013). Integrated vehicle dynamics control via coordination of active front steering and rear braking. *European Journal of Control*, 19(2), 121–143.

Fergani, S., Menhour, L., Sename, O., Dugard, L., and D'Andréa-Novel, B. (2016). LPV/H ∞ suspension robust control adaption of the dynamical lateral load transfers based on a differential algebraic estimation approach. In *8th IFAC International Symposium on Advances in Automotive Control (AAC 2016)*.

Karbalaei, R., Ghaffari, A., Kazemi, R., and Tabatabaei, S. (2007). A new intelligent strategy to integrated control of afs/dyc based on fuzzy logic. *International Journal of Mathematical, Physical and Engineering Sciences*, 1(1), 47–52.

Mirzaei, M. and Mirzaeinejad, H. (2017). Fuzzy scheduled optimal control of integrated vehicle braking and steering systems. *IEEE/ASME Transactions on Mechatronics*, 22(5), 2369–2379.

Poussot-Vassal, C., Sename, O., and Dugard, L. (2009). Robust vehicle dynamic stability controller involving steering and braking systems. In *IEEE European Control Conference (ECC)*, 3646–3651.

Rajamani, R. (2012). *Vehicle Dynamics and Control*. Springer.

Reznik, L. (1997). *Fuzzy controllers handbook: how to design them, how they work*. Elsevier.

Savaresi, S.M., Poussot-Vassal, C., Spelta, C., Sename, O., and Dugard, L. (2010). *Semi-active suspension control design for vehicles*. Elsevier.

Utkin, V. (2013). On convergence time and disturbance rejection of super-twisting control. *IEEE Transactions on Automatic Control*, 58(8), 2013–2017.

Vu, V.T., Sename, O., Dugard, L., and Gáspár, P. (2017). Enhancing roll stability of heavy vehicle by lqr active anti-roll bar control using electronic servo-valve hydraulic actuators. *Vehicle System Dynamics*, 55(9), 1405–1429.

Yao, J., Lv, G., Qv, M., Li, Z., Ren, S., and Taheri, S. (2017). Lateral stability control based on the roll moment distribution using a semiactive suspension. *Proceedings of the Institution of Mechanical Engineers, Part D: Journal of Automobile Engineering*, 231(12), 1627–1639.

Yoon, J., Yim, S., Cho, W., Koo, B., and Yi, K. (2010). Design of an unified chassis controller for rollover prevention, manoeuvrability and lateral stability. *Vehicle system dynamics*, 48(11), 1247–1268.

Appendix A. VEHICLE MODEL

$$g_\theta(X) = \frac{1}{I_x+M_s h_\theta^2}[\left(-F_{fr}+F_{fl}\right)t_f+\left(-F_{rr}+F_{rl}\right)t_r + M_s\left(h_\theta\ cos\left(\theta\right)+z\right)a_y + M_s\left(h_\theta\ sin\left(\theta\right)+z\right)g], \tag{A.1}$$

$$g_\phi(X) = \frac{1}{I_y+M_s h_\phi^2}[-\left(F_{fr}+F_{fl}\right)l_f+\left(F_{rr}+F_{rl}\right)l_r + M_s\left(h_\phi\ cos\left(\phi\right)+z\right)a_x + M_s\left(h_\phi\ sin\left(\phi\right)+z\right)g], \tag{A.2}$$

$$g_z(X) = \frac{1}{M_s}(F_{fr}+F_{fl}+F_{rr}+F_{rl}), \tag{A.3}$$

$$f_\theta = \frac{1}{I_x+M_s h_\theta^2}; f_\phi = \frac{1}{I_y+M_s h_\phi^2}; f_z = \frac{1}{M_s}, \tag{A.4}$$

$$g_\psi(X) = \tfrac{1}{I_z}[-t_f(F_{x,fl}-F_{x,fr})+l_f(F_{y,fl}+F_{y,fr}) - l_r(F_{y,rl}+F_{y,rr})-t_r(F_{x,rl}-F_{x,rr})], \tag{A.5}$$

$$f_{\psi,\delta}(X) = \frac{1}{I_z}[t_f(F_{y,fl}-F_{y,fr})+l_f(F_{x,fl}+F_{x,fr})], \tag{A.6}$$

$$f_{\psi,C_z} = \frac{1}{I_z}, \tag{A.7}$$

$$g_\beta(X) = (-1+\tfrac{l_r c_r-l_f c_f}{MV_x{}^2})(-\tfrac{l_f{}^2 c_f+l_r{}^2 c_r}{I_z V_x})\dot{\psi} + (-1+\tfrac{l_r c_r-l_f c_f}{MV_x{}^2})(\tfrac{l_r c_r-l_f c_f}{I_z})\beta+(-\tfrac{c_f+c_r}{MV_x})\dot{\beta}, \tag{A.8}$$

$$f_{\beta,\delta}(X) = (-1+\frac{l_r c_r-l_f c_f}{MV_x{}^2})\frac{l_f c_f}{I_z}, \tag{A.9}$$

$$f_{\beta,C_z}(X) = \frac{1}{I_z}(-1+\frac{l_r c_r-l_f c_f}{MV_x{}^2}). \tag{A.10}$$

F_{ij}, $F_{x,ij}$, and $F_{y,ij}$ are nonlinear functions of X detailed in Rajamani (2012).